

A Sparse Learning Approach to the Design of Radar Tunable Architectures with Enhanced Selectivity Properties

Sudan Han, Luca Pallotta, *Senior Member, IEEE*, Xiaotao Huang, *Member, IEEE*, Gaetano Giunta, *Senior Member, IEEE*, and Danilo Orlando, *Senior Member, IEEE*

Abstract—This paper considers the design of tunable decision schemes capable of rejecting with high probability mismatched signals embedded in Gaussian interference with unknown covariance matrix. To this end, a sparse recovery technique is exploited to enhance the resolution at which the target angle of arrival is estimated with the objective to obtain high-selective detectors. The outcomes of this estimation procedure are used to devise detection architectures relying on either the two-stage design paradigm or heuristic design procedures based upon the generalized likelihood ratio test. Remarkably, the new decision rules exhibit a bounded-constant false alarm rate property and allow for a tradeoff between the matched detection performance and the rejection of undesired signals by tuning a design parameter. At the analysis stage, the performance of the newly proposed detectors is assessed also in comparison with existing selective competitors. The results show that the new detectors can outperform the considered counterparts in terms of rejection of unwanted signals, while retaining reasonable detection performance of matched signals.

Index Terms—Adaptive radar detection, coherent interferers, constant false alarm rate, Gaussian interference, likelihood ratio test, mismatched signals, sidelobe signals, sparse recovery, tunable architectures, two-stage detectors.

I. INTRODUCTION

In the recent years, the design of adaptive detection architectures in the presence of mismatched signals has raised a strong interest in the radar community as corroborated by the multitude of contributions that can be found in the open literature [1]–[20]. As a matter of fact, in scenarios of practical interest, the direction of arrival of the signal backscattered from a target may be different from the nominal pointing direction of the mainbeam due to environmental and/or instrumental factors. For instance, in search mode, radar operates in situations where a possible target echoes could come from any arbitrary angle within the beamwidth with a consequent loss in detection performance and a biased estimate of the target direction. On the other hand, the presence of a coherent jammer or a strong target in the sidelobes (namely,

from a significantly mismatched direction of arrival) could trigger a detection which deceives the search system. Other causes of mismatched signals may be imperfect modeling of the mainlobe steering vector, multipath propagation, array calibration uncertainties, mutual coupling between the array elements, etc.

Conventional adaptive detection algorithms, namely those designed under the assumption of a perfect match between the nominal and the actual steering vector [21]–[27], behave quite differently in the presence of mismatched signals. Specifically, according to their directivity, defined as the capability of rejecting/detecting mismatched signals, they can be classified as [13]:

- robust decision schemes which provide good detection performances in the presence of echoes containing signal components not aligned with the nominal (transmitted) signal (see, for instance, the subspace detectors [28]–[30]);
- selective decision schemes which are capable of rejecting signals whose signature is unlikely to correspond to that of interest in order to avoid false alarms (see, for instance, [15], [18], [24], [31]).

From an operating point of view, selective detectors may be exploited to face with densely populated environments or to face with electronic countermeasures (coherent jammers) [32]. On the other hand, robust architectures are suitable to cover wide angular sectors by means of a low number of filters/pointing directions or to detect mismatched signals within the mainbeam. As corroborated by the numerous analysis in the presence of mismatched signals, generally speaking, an enhanced selectivity degrades the matched detection performance, whereas robust architectures can maintain good matched detection performance [14, and references therein]. Thus, it is clear that a decision scheme capable of modifying its behavior according to the specific scenario would offer a relevant flexibility in usage. This requirement has led to the birth of tunable detectors whose directivity can be set by means of suitable design parameters. Remarkably, they are capable of providing a good tradeoff between matched detection performance and rejection of unwanted signals.

There exist several design paradigms to come up with tunable architectures. A first approach consists in merging the decision statistics of existing detectors due to the inherent similarities between them [1]–[4]. As a result, the new

S. Han is with the National Innovation Institute of Defense Technology, Beijing, China E-mail: xiaoxiaosu0626@163.com.

L. Pallotta and G. Giunta are with Department of Engineering, University of Roma Tre, via Vito Volterra 62, 00146 Rome, Italy. E-mail: luca.pallotta@uniroma3.it, gaetano.giunta@uniroma3.it.

X. Huang is with the College of Electronic Science and Technology, National University of Defense Technology, Changsha 410073, China. E-mail: xthuang@nudt.edu.cn.

D. Orlando is with Università degli Studi “Niccolò Cusano”, via Don Carlo Gnocchi 3, 00166 Roma, Italy. E-mail: danilo.orlando@unicusano.it.

architecture encompasses the merged decision schemes as special cases by tuning suitable design parameters. Another class of tunable architectures can be formed by resorting to the theory of subspace detection. Specifically, at the design stage, it is assumed that the possible useful signals belong to a preassigned subspace of the observables or to a proper cone with the nominal steering vector as axis [5]–[7]. In these cases, the directivity can be modified by acting on the subspace properties or on the cone aperture. Finally, a powerful tool for the design of tunable architectures is the two-stage approach, which consists in cascading two decision schemes (usually with opposite behaviors in terms of directivity) [2], [8]–[13]. The overall detector decides for the alternative hypothesis if and only if the decision statistic of each stage is above the respective threshold. This scheme is tantamount to a logical AND between the two stages and it can be tuned by modifying the two thresholds. In fact, a preassigned value for the probability of false alarm (P_{fa}) can be maintained over different threshold pairs and, interestingly, each pair returns a specific directivity and matched detection performance [9], [10], [14].

In this paper, we focus on the design of tunable adaptive architectures capable of achieving an enhanced selectivity with respect to the state-of-the-art selective detectors while keeping good detection performance for matched signals embedded in Gaussian interference with unknown covariance matrix. To this end, we exploit sparse reconstruction techniques in conjunction with either the two-stage design paradigm or *ad hoc* modifications of the generalized likelihood ratio test (GLRT) [22]. More precisely, at the design stage, we take advantage of the inherent sparse nature of the signal model due to the fact that a large part of the angular sector under surveillance does not contain any signal of interest leading to a sparse scene. Therefore, we resort to the compressive sensing approach to estimate target response as well as its angle of arrival (AOA) [33]–[37] and use such estimates to build up two new classes of decision schemes. The first class is represented by two-stage architectures obtained by coupling the sparse amplitude detector (SAD), defined in Section IV, and classical constant false alarm rate (CFAR) detectors such as Kelly’s GLRT [21] or the adaptive matched filter (AMF) [22]. The second class of receivers is devised applying a heuristic procedure based upon the GLRT, where some parameters are assumed known and the others are estimated through the maximum likelihood approach possibly resorting to training samples collected in the proximity of the cell under test. Remarkably, it can be shown that the proposed architectures are bounded-CFAR.

It is important to notice that conversely to existing contributions on AOA estimation by means of sparse recovery, which focus on estimation aspects only and assume that the estimation algorithms are triggered by a preliminary detection stage [38]–[43], the newly proposed architectures jointly perform detection and estimation. In addition, the present approach allows us to tune the directivity of the proposed architectures through a design parameter used by the sparse estimation procedure leading to enhanced rejection capabilities of unwanted signals. The above issues appear for the first time (at least to the best of the authors’ knowledge) in this paper

and represent the main technical contribution.

The performance analysis is conducted over simulated data by comparing the proposed techniques with Kelly’s GLRT (which is considered as benchmark detector for matched signals), the AMF, and well-known selective architectures as the whitened adaptive beamformer orthogonal rejection test (W-ABORT) [15], the Rao test (RAO) [23], and the adaptive coherence estimator (ACE) [31] (also known as the adaptive normalized matched filter (ANMF) [44]). The illustrative examples point out that, at least for the considered simulation parameters, the newly proposed architectures are capable of exhibiting an increased selectivity with respect to the considered competitors and, at the same time, an excellent matched detection performance.

The remainder of the paper is organized as follows: Section II is devoted to the problem formulation. Section III describes the sparse recovery procedure. The proposed decision schemes based on the sparse estimates are devised in Section IV, while the performance of the new detectors is assessed in Section V. Finally, concluding remarks and future research tracks are given in Section VI.

A. Notation

Vectors and matrices are denoted by boldface lower-case and upper-case letters, respectively. The symbols $\det(\cdot)$, $\text{Tr}(\cdot)$, $(\cdot)^T$, and $(\cdot)^\dagger$ denote the determinant, trace, transpose, and conjugate transpose, respectively. As to numerical sets, \mathbb{R} is the set of real numbers, $\mathbb{R}^{N \times M}$ is the Euclidean space of $(N \times M)$ -dimensional real matrices (or vectors if $M = 1$), \mathbb{C} is the set of complex numbers, and $\mathbb{C}^{N \times M}$ is the Euclidean space of $(N \times M)$ -dimensional complex matrices (or vectors if $M = 1$). The Euclidean norm of a generic vector \mathbf{x} is denoted by $\|\mathbf{x}\|$. \mathbf{I}_N stands for the $N \times N$ identity matrix, while $\mathbf{0}$ is the null vector or matrix of proper size. Finally, given a vector \mathbf{a} , $\text{diag}(\mathbf{a})$ indicates the diagonal matrix whose i th diagonal element is the i th entry of \mathbf{a} .

II. PROBLEM FORMULATION AND MOTIVATION

Let us consider a search radar system which exploits a uniform linear array with N spatial channels and illuminates with its beam a given azimuth direction. The radar collects data from multiple range cells and tests whether or not the returns (from a specific range bin) contain a mainbeam target. In the positive case, it provides the AOA and the range measurement of the detected target. The classical detection procedure is implemented by testing range cell by range cell and it is often assumed that the actual target AOA coincides with the nominal steering angle (namely, the steering vector corresponding to the boresight). In this case, the detection problem at hand for a specific range bin, whose returns are collected in the vector $\mathbf{z} \in \mathbb{C}^{N \times 1}$, can be formulated in terms of the following hypothesis test

$$\begin{cases} H_1 : \mathbf{z} = \alpha \mathbf{v}(\theta_p) + \mathbf{n}, \\ H_0 : \mathbf{z} = \mathbf{n}, \end{cases} \quad (1)$$

where $\alpha \in \mathbb{C}$ accounts for transmitting antenna gain, the two-way path loss, and radar cross-section of the

(slowly-fluctuating) target, $\mathbf{n} \in \mathbb{C}^{N \times 1}$ represents the interference (clutter plus noise) component, modeled as a circular, zero-mean, complex Gaussian random vector with unknown positive-definite covariance matrix $\mathbf{R} \in \mathbb{C}^{N \times N}$, θ_p is the nominal AOA of the target (which coincides with the beamforming direction), and $\mathbf{v}(\theta_p) = [1, e^{j2\pi(d/\lambda)\sin(\theta_p)}, \dots, e^{j(N-1)2\pi(d/\lambda)\sin(\theta_p)}]^T \in \mathbb{C}^{N \times 1}$ is the nominal (spatial) steering vector with d the interelement spacing and λ the operating wavelength. When H_1 is declared, the range associated with \mathbf{z} and θ_p are returned as target parameter estimates. However, as mentioned in the previous section, in practice there exist several factors that would make the perfect match assumption between the signature of the received echoes and the nominal steering vector no longer valid. As a consequence, instead of problem (1), it would be more plausible to consider the following alternative

$$\begin{cases} H_1 : \mathbf{z} = \alpha \mathbf{v}(\theta_t) + \mathbf{n}, \\ H_0 : \mathbf{z} = \mathbf{n}, \end{cases} \quad (2)$$

where θ_t is the unknown AOA of the structured returns generated by an object in the surveillance area which may be different from the nominal pointing direction θ_p . Notice that such model is more general than (1) since it accounts for situations where the structured component of the collected vectors may be generated by noninterest objects as, for instance, a signal transmitted by a coherent jammer and entering from the sidelobes to inject false information into the radar processor [45]–[47]. Another example is represented by target-rich environments where an object within the 3 dB mainbeam but not aligned with the antenna boresight may trigger a detection [48]. In these operating scenarios, it would be desirable that the radar processor does not declare H_1 (see also antenna-based sidelobe blanking techniques [14], [45], [49]). Otherwise stated, the decision rules incorporated in the radar processor should be more inclined to decide for H_0 when the AOA of the coherent component is different from the nominal pointing direction on the basis of a mismatch degree decided by the user according to the specific application and the system operating requirements.

A viable strategy to cope with the above situations could be a sequential test of different mainbeam azimuth positions. In this context, assuming the availability of a secondary data set $\mathbf{z}_k \in \mathbb{C}^{N \times 1}$, $k = 1, \dots, K$, free of useful signal components but sharing the same spectral properties as the interference in \mathbf{z} (homogeneous environment), some classic decision rules can be used such as Kelly's GLRT [21] and the AMF [22], which ensure excellent matched detection performance. Specifically, for an angular position θ , the decision schemes for Kelly's GLRT and the AMF are given by

$$\Lambda_{\text{GLRT}} = \frac{|\mathbf{v}^\dagger(\theta) \widehat{\mathbf{R}}^{-1} \mathbf{z}|^2}{\left(\mathbf{v}^\dagger(\theta) \widehat{\mathbf{R}}^{-1} \mathbf{v}(\theta) \right) \left(K + \mathbf{z}^\dagger \widehat{\mathbf{R}}^{-1} \mathbf{z} \right)} \underset{H_0}{\overset{H_1}{>}} \eta_{\text{GLRT}}, \quad (3)$$

$$\Lambda_{\text{AMF}} = \frac{|\mathbf{v}^\dagger(\theta) \widehat{\mathbf{R}}^{-1} \mathbf{z}|^2}{\mathbf{v}^\dagger(\theta) \widehat{\mathbf{R}}^{-1} \mathbf{v}(\theta)} \underset{H_0}{\overset{H_1}{>}} \eta_{\text{AMF}}, \quad (4)$$

where $\widehat{\mathbf{R}} = \frac{1}{K} \sum_{k=1}^K \mathbf{z}_k \mathbf{z}_k^\dagger$ is the sample covariance matrix (SCM) over the training data, η_{GLRT} and η_{AMF} are the thresholds set in order to ensure a given P_{fa} . The relationships between the thresholds and the given P_{fa} are given by

$$\text{Kelly's GLRT: } \eta_{\text{GLRT}} = 1 - P_{fa}^{\frac{1}{K-N+1}}; \quad (5)$$

$$\text{AMF: } P_{fa} = \int_0^1 f_\beta(\rho; L+1, N-1) (1 + \eta_{\text{AMF}} \rho / K)^{-L} d\rho, \quad (6)$$

where $L = K - N + 1$ and

$$f_\beta(x; n, m) = \frac{(n+m-1)!}{(n-1)!(m-1)!} x^{n-1} (1-x)^{m-1} \quad (7)$$

is the complex central Beta probability density function (pdf) [21], [22]. Both Kelly's GLRT and the AMF ensure the CFAR property with respect to the interference covariance matrix. However, even though the performance in the case of matched signals is excellent, their azimuth discrimination as well as their capability of rejecting mismatched signals is limited. As a matter of fact, a target from directions that are different from the nominal pointing direction might trigger multiple detections (see [14] and references therein).

In order to circumvent this drawback, we devise two new classes of tunable architectures which take advantage of sparse reconstruction techniques to achieve an enhanced selectivity. More precisely, let us partition the angular region including the antenna mainbeam plus the relevant sidelobes into M uniformly spaced azimuth bins with separation $\Delta\theta$. Now, denoting by θ_l , $l = 1, \dots, M$, the angle corresponding to the center of the l th azimuth bin, we model the returns from a given range cell as follows

$$\mathbf{z} = \sum_{l=1}^M \alpha_l \mathbf{v}(\theta_l) + \mathbf{n} = \mathbf{V} \boldsymbol{\alpha} + \mathbf{n}, \quad (8)$$

$\mathbf{V} = [\mathbf{v}(\theta_1), \dots, \mathbf{v}(\theta_M)] \in \mathbb{C}^{N \times M}$ denotes the (so-called) dictionary matrix and $\boldsymbol{\alpha} = [\alpha_1, \dots, \alpha_M]^T \in \mathbb{C}^{M \times 1}$ is the vector whose entries are the responses of prospective targets.

Two remarks are now in order. First, note that $\boldsymbol{\alpha}$ is a sparse vector where the nonzero entry is that corresponding to the actual AOA of the target, whereas the other components are zero. Thus, (8) highlights the inherent sparse nature of the model under H_1 which allows to apply sparse reconstruction techniques [33]–[37], [50] to estimate $\boldsymbol{\alpha}$. Finally, as shown in what follows, it is important to underline that in this context, $\Delta\theta$ can be viewed as a tuning parameter by which it is possible to control the angular estimation resolution and the estimation quality. As a matter of fact, given $\Delta\theta$ (N), high values of N ($\Delta\theta$) allow for a low dictionary coherence leading to high quality estimation for the sparse recovery technique. In addition, under the above conditions, the inner product between adjacent columns of \mathbf{V} decreases and, consequently, the spillover of target energy between consecutive azimuth bins takes on low values. However, high values of $\Delta\theta$ decrease the angular resolution for the AOA estimation. Thus, establishing the range of values for $\Delta\theta$ is not an easy task and requires a preliminary analysis to find a good compromise

between estimation resolution and quality also accounting for the specific application and the system operating requirements.

In the next section, we describe the sparse recovery algorithm used to estimate α assuming that secondary data are available for the estimation of the interference covariance matrix and that $N < M$ in order to obtain an overdetermined model. Then, the above estimates are suitably exploited in Section IV to build up adaptive detection architectures with enhanced rejection capabilities of unwanted signals.

III. USER PARAMETER FREE BIC BASED SLIM (BSLIM) ALGORITHM

This section provides the description of the specific sparse recovery algorithm used to estimate α . Such algorithm relies on the sparse learning via iterative minimization (SLIM) method of [36]. This design choice is dictated by the fact that SLIM approach exhibits a computational cost similar to the widely used compressive sampling matching pursuit (CoSaMP) [51] but more accurate estimates than the latter, the iterative adaptive approach (IAA) [52], and matched filter techniques as shown in [36]. Moreover, the interested reader is referred to [53]–[58] for further applications/extensions of the SLIM.

In order to apply the SLIM method, we enforce a sparsity constraint on α using the same sparsity promoting prior pdf as in [36]:

$$f(\alpha) = \frac{1}{C} \prod_{l=1}^M \exp \left\{ -\frac{2}{q} (|\alpha_l|^q - 1) \right\}, \quad 0 < q \leq 1, \quad (9)$$

where C is a normalization constant which, without loss of generality, will be neglected in the sequel and q is a user parameter controlling the sparsity of α . In general, smaller q leads to sparser estimates in the framework of Bayesian inference [36]. The SLIM algorithm is based on a maximum a posteriori (MAP) approach, and thus given z and \mathbf{R} , the estimate of α can be written as

$$\hat{\alpha} = \arg \max_{\alpha} f(z|\alpha; \mathbf{R}) f(\alpha), \quad (10)$$

where

$$f(z|\alpha; \mathbf{R}) = \frac{1}{\pi^M \det(\mathbf{R})} \exp \left\{ -\left\| \mathbf{R}^{-1/2} (z - \mathbf{V}\alpha) \right\|^2 \right\} \quad (11)$$

is the conditional pdf of z given α . After some algebra, it is possible to show that (10) is tantamount to

$$\hat{\alpha} = \arg \min_{\alpha} g_q(\alpha, \mathbf{R}), \quad (12)$$

where

$$g_q(\alpha, \mathbf{R}) = \left\| \mathbf{R}^{-1/2} (z - \mathbf{V}\alpha) \right\|^2 + \sum_{l=1}^M \frac{2}{q} (|\alpha_l|^q - 1). \quad (13)$$

Before proceeding towards the solution of the above problem, we focus on the interference covariance matrix \mathbf{R} , that in practice is unknown. For this reason, the radar system collects training samples in proximity of that under test [59] and that are representative of the interference affecting the cell under test. Thus, in what follows, we estimate \mathbf{R} by means of the

SCM based on secondary data, namely $\hat{\mathbf{R}}$. As a consequence, after replacing \mathbf{R} with the considered estimate, problem (13) becomes

$$\hat{\alpha} = \arg \min_{\alpha} g_q(\alpha, \hat{\mathbf{R}}). \quad (14)$$

The last equation can be solved by setting to zero the first complex derivative of $g_q(\alpha, \hat{\mathbf{R}})$ with respect to α to obtain

$$-\mathbf{V}^\dagger \hat{\mathbf{R}}^{-1} z + \mathbf{V}^\dagger \hat{\mathbf{R}}^{-1} \mathbf{V} \alpha + \mathbf{P}^{-1} \alpha = 0, \quad (15)$$

where $\mathbf{P} = \mathbf{diag} ([|\alpha_1|^{2-q}, \dots, |\alpha_M|^{2-q}])$. Note that computing closed-form solution of the above equation is a difficult task because \mathbf{P} is a nonlinear function of α and, hence, we resort to an iterative method. Specifically, suppose that the estimate of α at the i th iteration, $\tilde{\alpha}^{(i)}$ say, is available, then \mathbf{P} in (15) can be computed as

$$\mathbf{P} = \tilde{\mathbf{P}}^{(i)} = \mathbf{diag} \left([|\tilde{\alpha}_1^{(i)}|^{2-q}, \dots, |\tilde{\alpha}_M^{(i)}|^{2-q}] \right). \quad (16)$$

Now, the estimate of α at the $(i+1)$ th iteration is obtained as follows

$$\tilde{\alpha}^{(i+1)} = \left[\mathbf{V}^\dagger \hat{\mathbf{R}}^{-1} \mathbf{V} + \left(\tilde{\mathbf{P}}^{(i)} \right)^{-1} \right]^{-1} \mathbf{V}^\dagger \hat{\mathbf{R}}^{-1} z. \quad (17)$$

As for the starting point of the above iterative procedure, we exploit the unconstrained ML estimate of the l th entry of α , namely

$$\tilde{\alpha}_l^{(0)} = \frac{\mathbf{v}^\dagger(\theta_l) \hat{\mathbf{R}}^{-1} z}{\mathbf{v}^\dagger(\theta_l) \hat{\mathbf{R}}^{-1} \mathbf{v}(\theta_l)}, \quad l = 1, \dots, M. \quad (18)$$

Simulation results, not reported here for brevity, have highlighted that for this specific problem, the SLIM algorithm almost shows no improvement after 15 iterations. For this reason, otherwise stated, all the next numerical examples are obtained using this number of iterations.

So far we have neglected the impact of q on $\tilde{\alpha}$, which clearly depends on the former and, hence, we denote this estimate by $\tilde{\alpha}_q$. The number of non-zero entries of $\tilde{\alpha}_q$ is generally larger than the actual number of targets, especially for large q . To further improve the sparsity of $\tilde{\alpha}_q$, the model-order selection Bayesian information criterion (BIC) can be incorporated into the procedure [60], [61]. Precisely, the BIC rule selects the order which minimizes the following objective function

$$\begin{aligned} \text{BIC}_q(h) &= -2 \ln f(z|\tilde{\alpha}_q(h); \hat{\mathbf{R}}) + 3h \log(2N) \\ &\approx 2 \left\| \hat{\mathbf{R}}^{-1/2} (z - \mathbf{V} \tilde{\alpha}_q(h)) \right\|^2 + 3h \log(2N), \end{aligned} \quad (19)$$

where h is an integer denoting the number of selected non-zero entries in $\tilde{\alpha}_q$ (the model order), $\tilde{\alpha}_q(h)$ is obtained from $\tilde{\alpha}_q$ setting to zero all the entries of $\tilde{\alpha}_q$ except the largest h values, and the coefficient 3 represents the number of unknown real-valued target parameters (complex amplitude and angle). Parameter h is assumed to belong to the finite set $\{1, \dots, h_{\max}\}$, where $h_{\max} \leq M$ is the maximum number of targets that are supposed to be present in the operating scenario. The specific h leading to the lowest BIC value is selected as an estimate of the actual number of targets for a given q . As a consequence, for each q , the amplitude vector estimate incorporating the

BIC algorithm and the corresponding BIC objective value are given by

$$\begin{aligned}\widehat{\alpha}_q &= \widetilde{\alpha}_q(\widehat{h}), \\ \text{BIC}_q &= \text{BIC}_q(\widehat{h}),\end{aligned}\quad (20)$$

respectively, where $\widehat{h} = \arg \min_h \text{BIC}_q(h)$. Summarizing, for a given q , the pseudocode of the BIC based SLIM (BSLIM) procedure is reported in Algorithm 1.

Algorithm 1 : Pseudocode of the BSLIM procedure

Input: Primary datum (cell under test) z , SCM $\widehat{\mathbf{R}}$, and dictionary matrix \mathbf{V} ;

Output: Amplitude vector estimate $\widehat{\alpha}_q$, and corresponding BIC objective value BIC_q ;

- 1: Initialize the amplitude vector using (18), denoted as $\widetilde{\alpha}_q^{(0)}$;
 - 2: Implement the iterative procedure according to (17) for $N_{\text{iteration}}$ times and denote the output as $\widetilde{\alpha}_q$;
 - 3: Compute BIC values for different $h \in \{1, \dots, h_{\max}\}$ using (19) and select the one leading to the lowest BIC value, denoted as \widehat{h} ;
 - 4: Update the amplitude vector estimate $\widehat{\alpha}_q$ and the corresponding value BIC_q resorting to (20).
-

As to the parameter q , we follow the lead of [36] by sampling the interval $(0, 1]$ to come up with a cardinality- Q set of admissible values for q , which is denoted as Ω . Then, for each $q \in \Omega$, the BSLIM procedure is carried out to obtain Q BIC values indicated as BIC_q , $q \in \Omega$. The optimal q value is then obtained as

$$\widehat{q} = \arg \min_{q \in \Omega} \text{BIC}_q. \quad (21)$$

Finally, the user parameter free amplitude vector estimate is given by

$$\widehat{\alpha} = \widehat{\alpha}_{\widehat{q}}. \quad (22)$$

The pseudocode of the user parameter free BSLIM algorithm is summarized in Algorithm 2.

Algorithm 2 : Pseudocode of the user parameter free BSLIM algorithm

Input: Primary datum (cell under test) z , SCM $\widehat{\mathbf{R}}$, and dictionary matrix \mathbf{V} ;

Output: Final sparse amplitude estimate $\widehat{\alpha}$;

- 1: Sample the interval $(0, 1]$ to come up with a cardinality- Q set of admissible values for q , denoted as $\Omega = \{q_1, \dots, q_Q\}$;
 - 2: For each element of Ω , implement the BSLIM procedure to get the amplitude vector estimate $\widehat{\alpha}_q$ and the corresponding BIC objective value BIC_q ;
 - 3: Select the specific q leading to the lowest BIC objective value and denote it as \widehat{q} ;
 - 4: Choose $\widehat{\alpha}_{\widehat{q}}$ as the final sparse amplitude estimate and denote it as $\widehat{\alpha}$.
-

IV. DECISION SCHEMES USING SPARSE AMPLITUDE ESTIMATION

This section addresses the design of decision strategies exploiting the sparse amplitude estimate. In this respect, a simple and intuitive way to perform the detection is to check the presence of a non-zero amplitude estimate indexed by m which, in turn, corresponds to the nominal pointing direction. To be more definite, denoting by $\widehat{\alpha}_m$ the entry of $\widehat{\alpha}$ related to the nominal steering angle, if $|\widehat{\alpha}_m| > 0$, then H_1 is declared. In the following, this decision strategy is referred to as SAD. However, due to the effect of estimation errors, the sparse amplitude estimate might be inaccurate and some of the non-zero elements might not represent the location of true targets. Besides, the SAD provides no control on the false alarm rate, which is an issue of primary concern in radar. In order to solve this problem, two classes of architectures are introduced in the following.

A. Decision Architectures Based on the Two-Stage Paradigm

The first class of architectures relies on the two-stage paradigm [14], [19]. Accordingly, the proposed detector is formed cascading two decision schemes and the final decision is taken by means of a logic AND between the two stages. In this context, we combine the SAD with classic CFAR detectors such as Kelly's GLRT and the AMF to obtain

$$\text{SAD-GLRT} : \begin{cases} H_0 : |\widehat{\alpha}_m| = 0 & \text{or } \Lambda_{\text{GLRT},m} < \eta_{\text{GLRT}} \\ H_1 : |\widehat{\alpha}_m| > 0 & \text{and } \Lambda_{\text{GLRT},m} > \eta_{\text{GLRT}} \end{cases}, \quad (23)$$

$$\text{SAD-AMF} : \begin{cases} H_0 : |\widehat{\alpha}_m| = 0 & \text{or } \Lambda_{\text{AMF},m} < \eta_{\text{AMF}} \\ H_1 : |\widehat{\alpha}_m| > 0 & \text{and } \Lambda_{\text{AMF},m} > \eta_{\text{AMF}} \end{cases}, \quad (24)$$

where we recall that m is the integer indexing the nominal pointing direction, $\Lambda_{\text{GLRT},m}$ and $\Lambda_{\text{AMF},m}$ are Kelly's GLRT and AMF decision statistics, respectively, evaluated using the nominal steering vector $\mathbf{v}(\theta_m)$, whereas η_{GLRT} and η_{AMF} are the detection thresholds for Kelly's GLRT and the AMF, respectively.

It is important to underline here that the actual P_{fa} of SAD-GLRT and SAD-AMF is given by

$$\begin{aligned}P_{fa,\text{SAD-GLRT}} &= P(|\widehat{\alpha}_m| > 0, \Lambda_{\text{GLRT},m} > \eta_{\text{GLRT}} | H_0) \\ &\leq P(\Lambda_{\text{GLRT},m} > \eta_{\text{GLRT}} | H_0),\end{aligned}\quad (25)$$

$$\begin{aligned}P_{fa,\text{SAD-AMF}} &= P(|\widehat{\alpha}_m| > 0, \Lambda_{\text{AMF},m} > \eta_{\text{AMF}} | H_0) \\ &\leq P(\Lambda_{\text{AMF},m} > \eta_{\text{AMF}} | H_0),\end{aligned}\quad (26)$$

and, hence, the SAD-GLRT and SAD-AMF are bounded CFAR since Kelly's GLRT and AMF are CFAR detectors.

B. Decision Architectures Based on the Likelihood Ratio Test

Another approach leading to detectors capable of controlling the false alarm rate consists in exploiting ad hoc modifications of the GLRT, where only some parameters are assumed unknown and estimated through the maximum likelihood approach, whereas the other parameters are replaced by suitable estimates. In this case, we can exploit the sparse amplitude estimates returned by the previously described estimation

procedure. To be more definite, let us denote by m the integer indexing the nominal steering direction, then the likelihood ratio test (LRT) is given by

$$\Lambda_{\text{LRT},m} = \frac{f(\mathbf{z}, \mathbf{z}_1, \dots, \mathbf{z}_K; \alpha_m, \mathbf{R}, H_1)}{f(\mathbf{z}, \mathbf{z}_1, \dots, \mathbf{z}_K; \mathbf{R}, H_0)} \underset{H_0}{\overset{H_1}{>}} \eta, \quad (27)$$

where

$$f(\mathbf{z}, \mathbf{z}_1, \dots, \mathbf{z}_K; \alpha_m, \mathbf{R}, H_1) = \left\{ \frac{\exp[-\text{Tr}(\mathbf{R}^{-1}\mathbf{T}_1)]}{\pi^N \det(\mathbf{R})} \right\}^{K+1} \quad (28)$$

and

$$f(\mathbf{z}, \mathbf{z}_1, \dots, \mathbf{z}_K; \mathbf{R}, H_0) = \left\{ \frac{\exp[-\text{Tr}(\mathbf{R}^{-1}\mathbf{T}_0)]}{\pi^N \det(\mathbf{R})} \right\}^{K+1} \quad (29)$$

with

$$\mathbf{T}_1 = \frac{1}{K+1} \left[(\mathbf{z} - \alpha_m \mathbf{v}(\theta_m))(\mathbf{z} - \alpha_m \mathbf{v}(\theta_m))^\dagger + K\hat{\mathbf{R}} \right] \quad (30)$$

and

$$\mathbf{T}_0 = \frac{1}{K+1} (\mathbf{z}\mathbf{z}^\dagger + K\hat{\mathbf{R}}) \quad (31)$$

are the joint pdfs of the vectors $\mathbf{z}, \mathbf{z}_1, \dots, \mathbf{z}_K$ under H_1 and H_0 , respectively. Note that by (27), the LRT for the nominal angular position is dependent on two unknown quantities, namely the target amplitude α_m and the interference covariance matrix \mathbf{R} .

1) *Case A (BSLIM-AMF)*: If we replace α_m and \mathbf{R} in (28)-(31) with the sparse estimate $\hat{\alpha}_m$ and the SCM $\hat{\mathbf{R}}$, respectively, then the logarithm of (27) can be written as

$$\begin{aligned} \Lambda_{\text{BSLIM-AMF},m} &= -(\mathbf{z} - \hat{\alpha}_m \mathbf{v}(\theta_m))^\dagger \hat{\mathbf{R}}^{-1} (\mathbf{z} - \hat{\alpha}_m \mathbf{v}(\theta_m)) \\ &\quad + \mathbf{z}^\dagger \hat{\mathbf{R}}^{-1} \mathbf{z} \underset{H_0}{\overset{H_1}{>}} \eta, \end{aligned} \quad (32)$$

which will be referred to in the following as BSLIM-AMF.

To gain some insight in (32), let us denote the unconstrained ML estimate of α_m for the single target scenario as

$$\hat{\alpha}_{\text{ML},m} = \frac{\mathbf{v}^\dagger(\theta_m) \hat{\mathbf{R}}^{-1} \mathbf{z}}{\mathbf{v}^\dagger(\theta_m) \hat{\mathbf{R}}^{-1} \mathbf{v}(\theta_m)}, \quad (33)$$

the decision statistic of (32) can be recast as

$$\begin{aligned} \Lambda_{\text{BSLIM-AMF},m} &= -(\mathbf{z} - \hat{\alpha}_m \mathbf{v}(\theta_m))^\dagger \hat{\mathbf{R}}^{-1} (\mathbf{z} - \hat{\alpha}_m \mathbf{v}(\theta_m)) + \mathbf{z}^\dagger \hat{\mathbf{R}}^{-1} \mathbf{z} \\ &= -\left(\mathbf{v}^\dagger(\theta_m) \hat{\mathbf{R}}^{-1} \mathbf{v}(\theta_m) \right) \left| \hat{\alpha}_m - \frac{\mathbf{v}^\dagger(\theta_m) \hat{\mathbf{R}}^{-1} \mathbf{z}}{\mathbf{v}(\theta_m)^\dagger \hat{\mathbf{R}}^{-1} \mathbf{v}(\theta_m)} \right|^2 \\ &\quad + \frac{|\mathbf{v}^\dagger(\theta_m) \hat{\mathbf{R}}^{-1} \mathbf{z}|^2}{\mathbf{v}^\dagger(\theta_m) \hat{\mathbf{R}}^{-1} \mathbf{v}(\theta_m)} \\ &= \Lambda_{\text{AMF},m} - \left(\mathbf{v}^\dagger(\theta_m) \hat{\mathbf{R}}^{-1} \mathbf{v}(\theta_m) \right) |\hat{\alpha}_m - \hat{\alpha}_{\text{ML},m}|^2 \\ &= \Lambda_{\text{AMF},m} \left(1 - \frac{|\hat{\alpha}_m - \hat{\alpha}_{\text{ML},m}|^2}{|\hat{\alpha}_{\text{ML},m}|^2} \right). \end{aligned} \quad (34)$$

where $\Lambda_{\text{AMF},m}$ is the AMF decision statistic evaluated with the steering vector $\mathbf{v}(\theta_m)$. The only difference between the decision statistics of BSLIM-AMF and AMF lies on the multiplier $(1 - |\hat{\alpha}_m - \hat{\alpha}_{\text{ML},m}|^2/|\hat{\alpha}_{\text{ML},m}|^2)$. For matched or slightly mismatched signals and high signal-to-interference-plus-noise-ratio (SINR), both of $\hat{\alpha}_m$ and $\hat{\alpha}_{\text{ML},m}$ approach the true amplitude, and thus the BSLIM-AMF tends to the AMF. In contrast, for highly mismatched signals, $\hat{\alpha}_m$ normally equals to zero (namely, $\Lambda_{\text{BSLIM-AMF},m} = 0$) whereas $\Lambda_{\text{AMF},m}$ might be large. This observation suggests that the BSLIM-AMF should outperform AMF in terms of rejecting unwanted signals.

2) *Case B (BSLIM-GLRT)*: Following the lead of Kelly's GLRT, it is possible to show that

$$\begin{aligned} \max_{\mathbf{R}} \Lambda_{\text{LRT},m} &= \left\{ \frac{\det(\mathbf{T}_0)}{\det(\mathbf{T}_1)} \right\}^{K+1} \\ &= \left\{ \frac{K + \mathbf{z}^\dagger \hat{\mathbf{R}}^{-1} \mathbf{z}}{K + (\mathbf{z} - \alpha_m \mathbf{v}(\theta_m))^\dagger \hat{\mathbf{R}}^{-1} (\mathbf{z} - \alpha_m \mathbf{v}(\theta_m))} \right\}^{K+1}. \end{aligned} \quad (35)$$

Using the sparse estimate $\hat{\alpha}_m$ in place of α_m and taking the $(K+1)$ st root, we obtain the following decision rule

$$\frac{K + \mathbf{z}^\dagger \hat{\mathbf{R}}^{-1} \mathbf{z}}{K + \mathbf{z}^\dagger \hat{\mathbf{R}}^{-1} \mathbf{z} - \Lambda_{\text{BSLIM-AMF},m}} \underset{H_0}{\overset{H_1}{>}} \eta, \quad (36)$$

which is statistically equivalent to

$$\begin{aligned} \Lambda_{\text{BSLIM-GLRT},m} &= \frac{\Lambda_{\text{BSLIM-AMF},m}}{K + \mathbf{z}^\dagger \hat{\mathbf{R}}^{-1} \mathbf{z}} \\ &= \Lambda_{\text{GLRT},m} \left(1 - \frac{|\hat{\alpha}_m - \hat{\alpha}_{\text{ML},m}|^2}{|\hat{\alpha}_{\text{ML},m}|^2} \right) \underset{H_0}{\overset{H_1}{>}} \eta. \end{aligned} \quad (37)$$

The above architectures is referred to as BSLIM-GLRT. Similarly, the BSLIM-GLRT differs from Kelly's GLRT only by the multiplier $(1 - |\hat{\alpha}_m - \hat{\alpha}_{\text{ML},m}|^2/|\hat{\alpha}_{\text{ML},m}|^2)$.

As a final remark, note that the left hand side of (32) and (37) are upper bounded by the AMF and Kelly's GLRT decision statistics, respectively, the BSLIM-AMF and BSLIM-GLRT are also bounded CFAR.

The block-schemes of the proposed decision architectures are depicted in Fig. 1.

V. NUMERICAL EXAMPLES

In this section, we focus on the performance assessment of the SAD-AMF, SAD-GLRT, BSLIM-AMF, and BSLIM-GLRT, also in comparison with well-known selective decision schemes. Since closed-form expressions for the P_{fa} and the probability of detection (P_d) are not available for the new detectors, we evaluate them resorting to standard Monte Carlo techniques based on $1000/P_{fa}$ and 10^4 independent trials, respectively. The interference is modeled as an exponentially-correlated complex Gaussian vector with one-lag correlation coefficient ρ , namely the (i, j) th element of the covariance matrix \mathbf{R} is given by $\rho^{|i-j|}$, $i, j = 1, \dots, N$, with $\rho = 0.95$. Finally, the interelement spacing, namely d , is set to $\lambda/2$, $h \in \{1, \dots, M\}$, and $q \in \Omega = \{0.01, 0.1, 0.2, \dots, 1\}$.

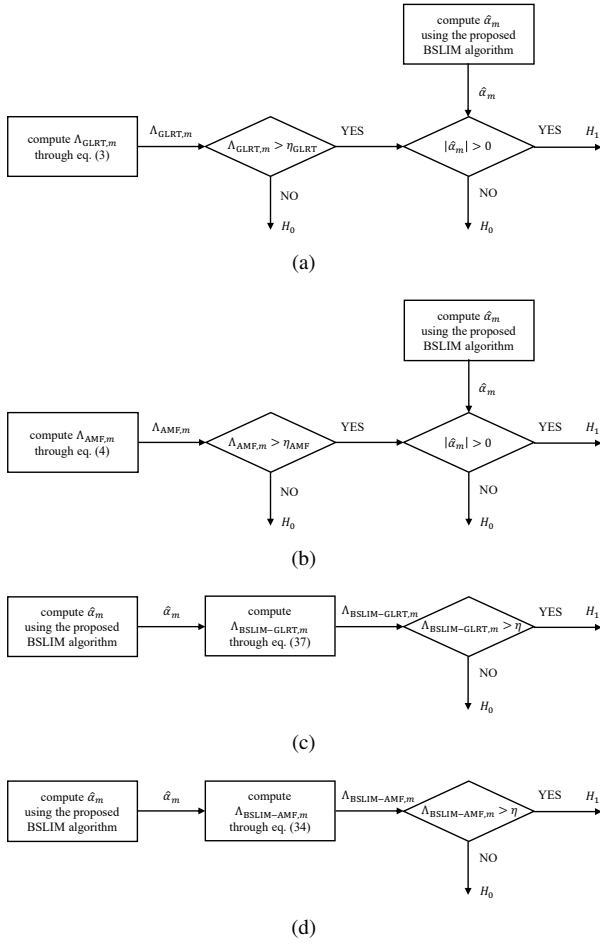


Fig. 1: Block schemes of the proposed decision architectures. (a) Two-stage detector based upon Kelly's GLRT. (b) Two-stage detector based upon the AMF. (c) One-stage detector based upon the GLRT. (d) One-stage detector based upon the AMF.

A. P_{fa} analysis

In Figs. 2 to 4, the P_{fa} behavior of the new decision schemes is studied assuming that $N = 8$ and the nominal pointing direction is 0° . The angular region corresponding to the dictionary ranges from -48° to 48° in order to include the mainbeam (whose 3 dB beamwidth is about 8.66° and four sidelobes (two sidelobes on the left and two sidelobes on the right). Exploiting the bounded CFAR property, the thresholds in (23), (24), (32) and (37) are set equal to those of the AMF and Kelly's GLRT, respectively. Precisely, the thresholds in (23) and (37) are set equal to η_{GLRT} , which is calculated according to (5) whereas the thresholds in (24) and (32) are set to η_{AMF} , which is computed resorting to (6). Besides, P_{fa} is set to 10^{-3} in order to limit the computational burden. Fig. 2 shows the actual P_{fa} versus the number of iterations $N_{iteration}$ used in the BSLIM procedure for $K = 32$ and $\Delta\theta = 3^\circ$ (namely, $M = 33$). The curves confirm that all the new decision rules possess the bounded CFAR property. Moreover, for the chosen parameters, the P_{fa} value of them almost keeps unaltered when $N_{iteration} \geq 11$.

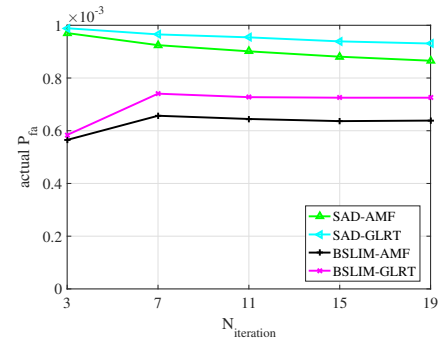


Fig. 2: Actual P_{fa} versus $N_{iteration}$ for $N = 8$, $K = 32$, and $\Delta\theta = 3^\circ$.

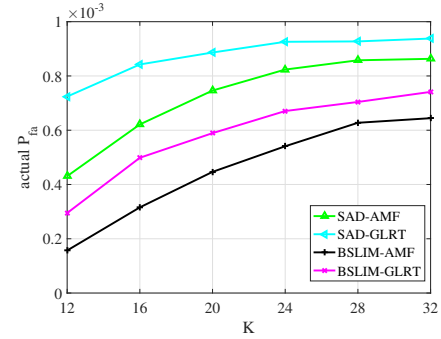


Fig. 3: Actual P_{fa} versus K for $N = 8$, $\Delta\theta = 3^\circ$, and $N_{iteration} = 15$.

The P_{fa} values versus $N_{iteration}$ for other parameters have been also evaluated. Such simulations, not reported here for brevity, highlight that the P_{fa} value for the considered decision schemes almost shows no changes when $N_{iteration} \geq 15$. The bounded CFAR property of the new decision architectures is further validated in Fig. 3, where the actual P_{fa} versus K is plotted for $\Delta\theta = 3^\circ$ and $N_{iteration} = 15$. The plot shows that larger K generally leads to P_{fa} values closer and closer to the nominal P_{fa} value and the P_{fa} behavior shows small changes when K is sufficiently large. Furthermore, for a given K , the P_{fa} value of the SAD-GLRT is the closest to the nominal one among the considered detectors while that of the BSLIM-AMF exhibits the greatest deviation. Fig. 4 plots

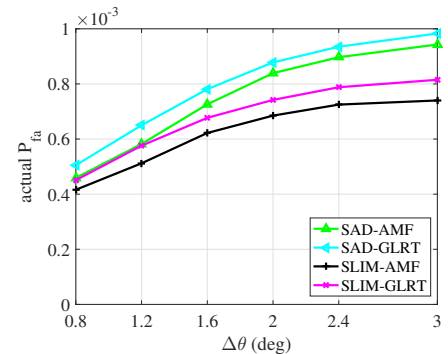


Fig. 4: Actual P_{fa} versus $\Delta\theta$ for $N = 8$, $K = 32$, and $N_{iteration} = 15$.

the actual P_{fa} versus $\Delta\theta$ for $K = 32$ and $N_{iteration} = 15$. The curves point out that the estimated P_{fa} value approaches the nominal P_{fa} value as $\Delta\theta$ increases. It is worth noticing that the P_{fa} deviation is generally smaller than one order of magnitude, i.e., $0.1 \times$ nominal P_{fa} value. As a consequence, in practical applications, the angular separation $\Delta\theta$ could be properly selected in order to ensure that the P_{fa} deviation is smaller than the maximum tolerable value.

B. P_d analysis

In the sequel, the P_d behavior of the proposed decision schemes is analyzed for both matched and mismatched signals assuming $P_{fa} = 10^{-3}$, the nominal pointing direction is 0° and $N_{iteration} = 15$, also in comparison with the AMF [22], Kelly's GLRT [21], the Rao detector (RAO) [23], the W-ABORT [15], and the ACE [31], [44]. For the reader ease, the expressions of the RAO, the W-ABORT, and the ACE are given by

$$\Lambda_{\text{RAO}} = \frac{|\mathbf{v}^\dagger(\theta_m) \widehat{\mathbf{S}}_1^{-1} \mathbf{z}|^2}{\mathbf{v}^\dagger(\theta_m) \widehat{\mathbf{S}}_1^{-1} \mathbf{v}(\theta_m)}, \quad (38)$$

$$\Lambda_{\text{WA}} = \frac{\left(K + \mathbf{z}^\dagger \widehat{\mathbf{R}}^{-1} \mathbf{z} \right)^{-1}}{\left[1 - \frac{|\mathbf{v}^\dagger(\theta_m) \widehat{\mathbf{R}}^{-1} \mathbf{z}|^2}{\left(\mathbf{v}^\dagger(\theta_m) \widehat{\mathbf{R}}^{-1} \mathbf{v}(\theta_m) \right) \left(K + \mathbf{z}^\dagger \widehat{\mathbf{R}}^{-1} \mathbf{z} \right)} \right]^2}, \quad (39)$$

and

$$\Lambda_{\text{ACE}} = \frac{|\mathbf{v}^\dagger(\theta_m) \widehat{\mathbf{R}}^{-1} \mathbf{z}|^2}{\left(\mathbf{v}^\dagger(\theta_m) \widehat{\mathbf{R}}^{-1} \mathbf{v}(\theta_m) \right) \left(\mathbf{z}^\dagger \widehat{\mathbf{R}}^{-1} \mathbf{z} \right)}, \quad (40)$$

respectively, where $\widehat{\mathbf{S}}_1 = \mathbf{z} \mathbf{z}^\dagger + K \widehat{\mathbf{R}}$. According to the decision rules (23), (24), (34) and (37), the detection performance is affected by the sparse amplitude estimate. The latter is dependent on the following parameters: the dictionary \mathbf{V} (including the number of columns M , the size of each column N and the angular separation between adjacent columns $\Delta\theta$), the interference covariance matrix \mathbf{R} , the number of secondary data K , the true target angle θ_t , and the SINR, which is defined as

$$\text{SINR} = |\alpha|^2 \mathbf{v}(\theta_t)^\dagger \mathbf{R}^{-1} \mathbf{v}(\theta_t), \quad (41)$$

where we recall that θ_t is the actual AOA of the target. Moreover, for a specific target, the P_d value obtained using the SAD-AMF and BSLIM-AMF is smaller than or equal to that of the AMF, whereas the upper bound for the P_d of SAD-GLRT and BSLIM-GLRT is represented by that of Kelly's GLRT.

It is now worth to underline that as claimed in [62], typically, to obtain a satisfactory sparse amplitude estimate exploiting sparse recovery algorithms, under the additive white Gaussian noise assumption, the dictionary is required to meet some requirements such as the restricted isometry property (RIP) or low coherence. The signal model (8) in Section II can be transformed by whitening with respect to the interference covariance matrix, namely

$$\mathbf{z}_w = \mathbf{V}_w \boldsymbol{\alpha} + \mathbf{n}_w, \quad (42)$$

where $\mathbf{V}_w = \mathbf{R}^{-1/2} \mathbf{V}$ and $\mathbf{n}_w = \mathbf{R}^{-1/2} \mathbf{n}$ represent the whitened dictionary and interference component, respectively. As a consequence, the coherence of the dictionary is given by [62]

$$\begin{aligned} \mu(\mathbf{V}_w) &= \arg \max_{1 \leq i, j \leq M, i \neq j} \left| \frac{\mathbf{v}_{w,i}^\dagger \mathbf{v}_{w,j}}{\|\mathbf{v}_{w,i}\| \|\mathbf{v}_{w,j}\|} \right| \\ &= \arg \max_{1 \leq i, j \leq M, i \neq j} \left| \frac{\mathbf{v}_i^\dagger \mathbf{R}^{-1} \mathbf{v}_j}{\|\mathbf{R}^{-1/2} \mathbf{v}_i\| \|\mathbf{R}^{-1/2} \mathbf{v}_j\|} \right|, \end{aligned} \quad (43)$$

where $\mathbf{v}_{w,i}$ and \mathbf{v}_i , $i = 1, \dots, M$, denote the i th column of \mathbf{V}_w and \mathbf{V} , respectively. In addition, the coherence corresponding to the m th azimuth bin can be defined as

$$\mu(\mathbf{V}_w, \theta_m) = \arg \max_{\substack{1 \leq i \leq M \\ \mathbf{v}_i \neq \mathbf{v}(\theta_m)}} \left| \frac{\mathbf{v}_i^\dagger \mathbf{R}^{-1} \mathbf{v}(\theta_m)}{\|\mathbf{R}^{-1/2} \mathbf{v}_i\| \|\mathbf{R}^{-1/2} \mathbf{v}(\theta_m)\|} \right|. \quad (44)$$

In order to obtain a good estimate of α_m , $m = 1, \dots, M$, $\mu(\mathbf{V}_w, \theta_m)$ should be small.

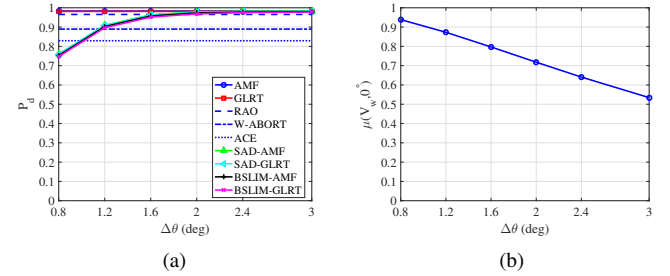


Fig. 5: P_d behavior and $\mu(\mathbf{V}_w, 0^\circ)$ versus $\Delta\theta$ for $N = 8$, $K = 32$, $\text{SINR} = 14$ dB, and $\theta_t = 0^\circ$. (a) P_d . (b) $\mu(\mathbf{V}_w, 0^\circ)$.

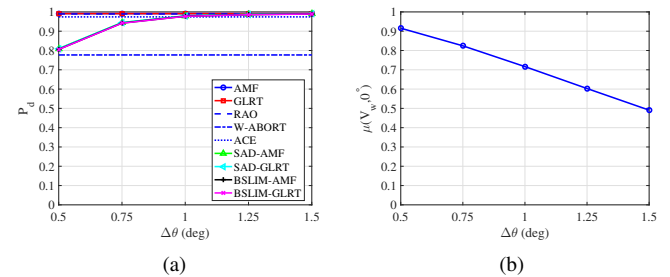


Fig. 6: P_d behavior and $\mu(\mathbf{V}_w, 0^\circ)$ versus $\Delta\theta$ for $N = 24$, $K = 96$, $\text{SINR} = 14$ dB, and $\theta_t = 0^\circ$. (a) P_d . (b) $\mu(\mathbf{V}_w, 0^\circ)$.

Figs. 5 to 8 study P_d under the perfect matching condition, namely, the true target angle coincides with the nominal pointing direction. In particular, Fig. 5 plots P_d versus $\Delta\theta$ for $N = 8$, $K = 32$, and $\text{SINR} = 14$ dB. The coherence corresponding to the nominal pointing angle $\mu(\mathbf{V}_w, 0^\circ)$ computed according to (44) is also provided. The plots highlight that, for the considered parameters, the best performance is achieved by the AMF, Kelly's GLRT and RAO and their P_d value is approximately 1 whereas the P_d values for W-ABORT and ACE are 0.89 and 0.83, respectively. In contrast, the P_d

value of the new detectors increases as $\Delta\theta$ increases. This is due to the fact that the lower the coherence, the more accurate the sparse amplitude estimate and thus improved P_d performance can be achieved. Moreover, the SAD-AMF, SAD-GLRT, BSLIM-AMF and BSLIM-GLRT almost share the same performance¹. In Fig. 6, P_d and coherence are plotted versus $\Delta\theta$ for $N = 24$, $K = 96$, and SINR = 14 dB. In this situation, the selected angular region, again including the mainbeam (whose 3 dB beamwidth is now about 2.88°) and four sidelobes, ranges from -15° to 15° . The plots highlight that for a fixed $\Delta\theta$, a larger value of N leads to a smaller value of $\mu(\mathbf{V}_w, 0^\circ)$. Besides, for this specific case, P_d loss of the proposed strategies (the loss of the new detectors as compared to their respective counterparts, i.e., AMF for SAD-AMF and BSLIM-AMF, Kelly's GLRT for SAD-GLRT and BSLIM-GLRT) approximately reaches 0 when $\Delta\theta \geq 1.5$ (namely, $\mu(\mathbf{V}_w, 0^\circ) \leq 0.4909$). Additional experiments have been conducted for other parameter settings, whose results are not reported here for brevity, and the results confirm that when $\mu(\mathbf{V}_w, 0^\circ) \leq 0.5$ and $K \geq 4N$, the SAD-AMF, SAD-GLRT, BSLIM-AMF and BSLIM-GLRT almost ensure the same performance as their respective counterparts.

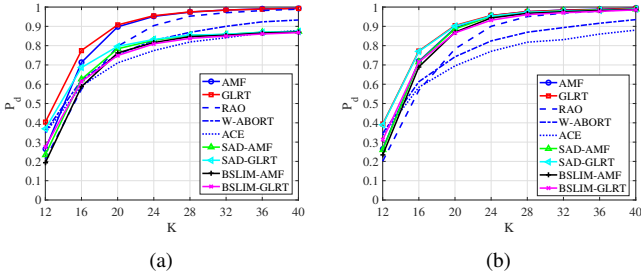


Fig. 7: P_d versus K for $N = 8$, SINR = 14 dB, $\theta_t = 0^\circ$ and different $\Delta\theta$ values. (a) $\Delta\theta = 1^\circ$. (b) $\Delta\theta = 2^\circ$.

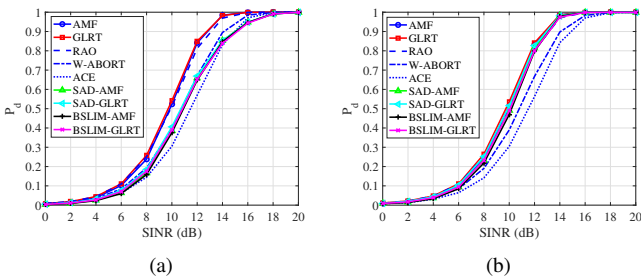


Fig. 8: P_d versus SINR for $N = 8$, $K = 32$, $\theta_t = 0^\circ$ and two values of $\Delta\theta$. (a) $\Delta\theta = 1^\circ$. (b) $\Delta\theta = 2^\circ$.

In Fig. 7, the effects of K on P_d are analyzed, to this end, P_d versus K is plotted for $N = 8$ and SINR = 14 dB. Two values of $\Delta\theta$ are considered: (a) $\Delta\theta = 1^\circ$; (b) $\Delta\theta = 2^\circ$. The plots highlight that for all the detectors, the larger the K ,

¹This is not a general case. Simulations highlight that the behavior of the four considered decision schemes might exhibit a significant gap when K is small (see, for instance, Fig. 7).

the better the P_d . Moreover, for $K \geq 4N$, the AMF, Kelly's GLRT and RAO approximately share the same performance whereas SAD-AMF, SAD-GLRT, BSLIM-AMF and BSLIM-GLRT curves are clustered together. Finally, for the SAD-AMF, SAD-GLRT, BSLIM-AMF and BSLIM-GLRT, when the coherence is high (case (a)), the P_d loss is generally non negligible. In contrast, when the coherence is sufficiently low (case (b)), the performance degradation is usually acceptable. As a consequence, to ensure a good detection performance for matched signals, the coherence should be low. This property is further confirmed in Fig. 8, where P_d versus SINR for $N = 8$, $K = 32$, and two values of $\Delta\theta$: (a) $\Delta\theta = 1^\circ$; (b) $\Delta\theta = 2^\circ$ is plotted.

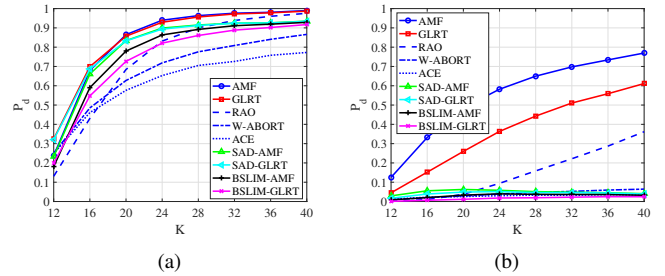


Fig. 9: P_d versus K for $N = 8$, $\Delta\theta = 2^\circ$, SINR = 14 dB and two θ_t values. (a) $\theta_t = 0.5^\circ$. (b) $\theta_t = 2^\circ$.

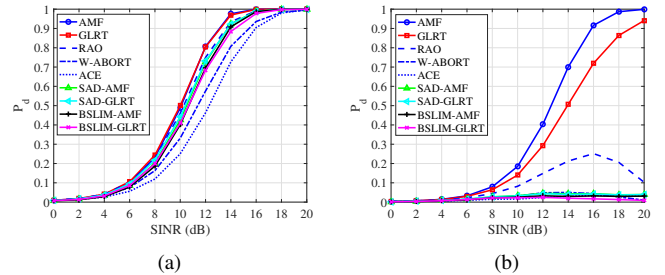


Fig. 10: P_d versus SINR for $N = 8$, $K = 32$, $\Delta\theta = 2^\circ$, and two θ_t values. (a) $\theta_t = 0.5^\circ$. (b) $\theta_t = 2^\circ$.

The last part of the analysis focuses on the case of mismatched signals, where the actual angle of the coherent component is not aligned with the (nominal) angle under test. The next numerical examples are aimed at showing that the proposed architectures can ensure an enhanced selectivity. As in the case of matched targets, the influence of K and SINR is assessed. Specifically, in Fig. 9, P_d versus K is plotted for $N = 8$, $\Delta\theta = 2^\circ$, SINR = 14 dB and two values of θ_t : (a) $\theta_t = 0.5^\circ$ (the angle of the target is not aligned with any value of θ_m , $m = 1, \dots, M$, where θ_m is the m th angular position among the discretized antenna beam); (b) $\theta_t = 2^\circ$ (the angle of the target coincides with a specific value of θ_m but is not equal to the nominal angle). The plots highlight that for the chosen parameters, the SAD-AMF, SAD-GLRT, BSLIM-AMF, and BSLIM-GLRT significantly outperform the AMF and Kelly's GLRT in terms of rejecting mismatched signals for a mismatch of 2° . Moreover, the P_d difference between

the proposed four decision schemes and the AMF and Kelly's GLRT grows as K increases for case (b). Precisely, for case (b), the P_d value of the SAD-AMF, SAD-GLRT, BSLIM-AMF and BSLIM-GLRT is always smaller than 0.1 for all the values of K . In contrast, the P_d values of the AMF and Kelly's GLRT are 0.32 and 0.15 respectively when $K = 16$, whereas 0.77 and 0.6 respectively when $K = 40$.

The improved capability of rejecting mismatched signals for the proposed four detectors is further confirmed in Fig. 10, where P_d versus SINR is plotted for $N = 8$, $K = 32$, $\Delta\theta = 2^\circ$, and the same values of θ_t as in Fig. 9. The plots highlight that for the AMF and Kelly's GLRT, the P_d value increases as SINR increases. On the other hand, for SAD-AMF, SAD-GLRT, BSLIM-AMF, and BSLIM-GLRT, the P_d value increases as SINR increases for case (a) whereas shows small changes for case (b). This is due to the fact that for case (b), the estimated target angular position (i.e., the non-zero element in $\hat{\alpha}$) exploiting the user parameter free BSLIM procedure is with high probability not aligned with the nominal angle.

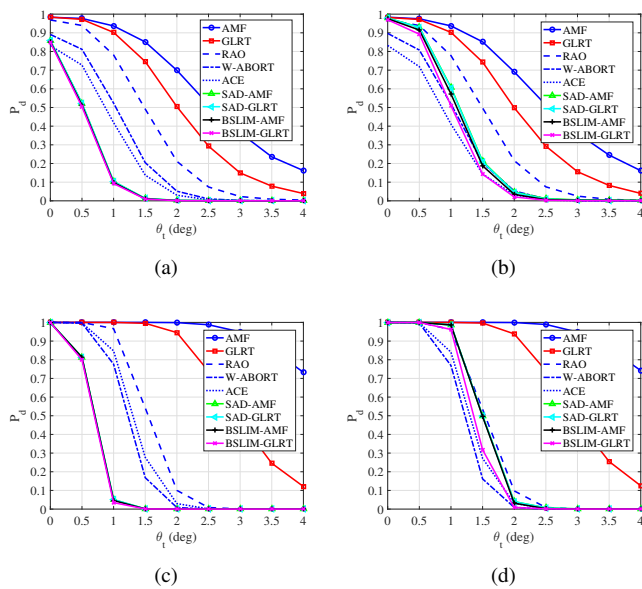


Fig. 11: P_d versus θ_t for $N = 8$ and $K = 32$. (a) $\Delta\theta = 1^\circ$ and SINR = 14 dB. (b) $\Delta\theta = 2^\circ$ and SINR = 14 dB. (c) $\Delta\theta = 1^\circ$ and SINR = 20 dB. (d) $\Delta\theta = 2^\circ$ and SINR = 20 dB.

Fig. 11 provides the P_d curves as functions of θ_t , namely the actual azimuthal angle θ_t of the coherent component, assuming $N = 8$, $K = 32$, two values of SINR and $\Delta\theta$. The curves show that the ACE and W-ABORT outperform the AMF, Kelly's GLRT and RAO in terms of selectivity, whereas the new decision schemes can provide an excellent capability of rejecting undesired signals by properly selecting the value of $\Delta\theta$ as shown in subfigures (a) and (c). The mismatched signal detection performance of SAD-GLRT and BSLIM-GLRT in comparison with those of the ACE and the W-ABORT are also analyzed in Fig. 12 for $\Delta\theta = 1^\circ$, wherein the contours of constant P_d are represented as a

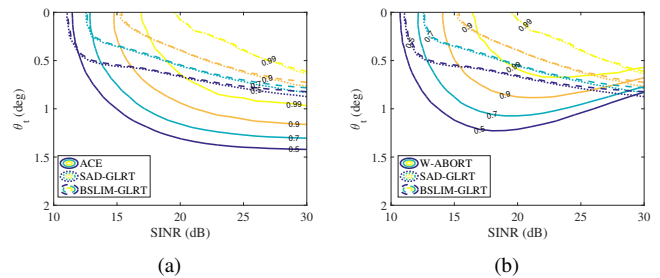


Fig. 12: Contours of constant P_d for $N = 8$, $K = 32$, and $\Delta\theta = 1^\circ$. (a) ACE, SAD-GLRT and BSLIM-GLRT. (b) W-ABORT, SAD-GLRT and BSLIM-GLRT.

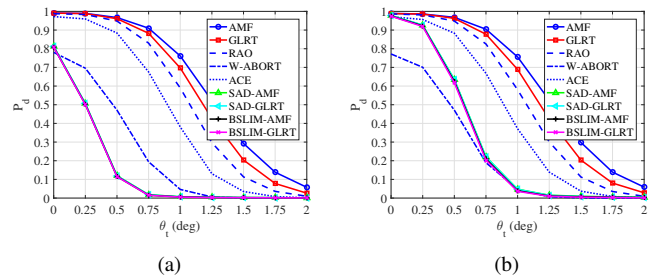


Fig. 13: P_d versus θ_t for $N = 24$, $K = 96$, SINR = 14 dB and two values of $\Delta\theta$. (a) $\Delta\theta = 0.5^\circ$. (b) $\Delta\theta = 1^\circ$.

function of the mismatch angle, plotted vertically, and the SINR, plotted horizontally². It is noted that the SAD-AMF and BSLIM-AMF almost exhibit the same performance as the SAD-GLRT and BSLIM-GLRT, whose curves are not shown here for clarity. The figure highlights that the SAD-GLRT, BSLIM-GLRT, ACE, and W-ABORT share approximately the same performance for $\theta_t = 0^\circ$, but the contours of SAD-GLRT and BSLIM-GLRT are more compressed towards zero with respect to those of the ACE and the W-ABORT. The quid pro quo for this enhanced selectivity is a performance degradation for matched signals with respect to Kelly's GLRT, the AMF, and RAO as shown in Fig. 8. Nevertheless, the other selective architectures share more or less the same matched detection performance as the new decision schemes. Moreover, increasing $\Delta\theta$ reduces the selectivity but restores the matched detection performance. As a matter of fact, for $\Delta\theta = 2^\circ$ (subfigures (b) and (d) in Fig. 11), the new architectures are slightly less selective than the ACE and the W-ABORT, but the latter experience a nonnegligible loss in matched detection performance with respect to the former as corroborated by Fig. 8. This behavior is further confirmed in Fig. 13, where P_d versus θ_t is plotted for $N = 24$, $K = 96$, SINR = 14 dB and two values of $\Delta\theta$. Comparing Fig. 11 and Fig. 13, it is clear that for a given SINR, the capability of distinguishing targets whose angles are close each other improves as N increases.

Summarizing, a suitable selection of $\Delta\theta$ for the SAD-AMF, SAD-GLRT, BSLIM-AMF and BSLIM-GLRT allows for a

²Similar 2-dimensional plots were introduced in [18], where they are referred to as mesa plots.

tradeoff between the detection of matched targets and rejection of undesired signals.

VI. CONCLUSION

In this paper, we have considered the design of tunable detectors based on sparse recovery techniques in order to achieve an enhanced selectivity assuming colored Gaussian interference with unknown covariance matrix. In this context, we have introduced a user parameter free sparse recovery algorithm inspired by the SLIM method [36]. Then, the estimates provided by the latter procedure have been used to devise two classes of detectors resorting to either the two-stage detection theory (leading to the SAD-AMF and the SAD-GLRT) or heuristic modifications of the GLRT (giving rise to the BSLIM-AMF and the BSLIM-GLRT). Moreover, we have proved that the new decision architectures exhibit a bounded-CFAR behavior. Simulation results have validated that the new detectors can outperform the conventional decision schemes in terms of selectivity by properly choosing the value of the tuning parameter $\Delta\theta$. Possible future research directions might concern the extensions of the proposed framework to range-spread targets as well as to non-Gaussian interference. Finally, it would be interesting to test the proposed detectors also on real recorded data.

ACKNOWLEDGMENT

The authors would like to thank Prof. A. De Maio for the exciting and interesting discussions.

REFERENCES

- [1] S. Z. Kalson, "An adaptive array detector with mismatched signal rejection," *IEEE Transactions on Aerospace and Electronic Systems*, vol. 28, no. 1, pp. 195–207, Jan 1992.
- [2] F. Bandiera, D. Orlando, and G. Ricci, "One- and two-stage tunable receivers," *IEEE Transactions on Signal Processing*, vol. 57, no. 8, pp. 3264–3273, Aug 2009.
- [3] C. Hao, B. Liu, S. Yan, and L. Cai, "Parametric adaptive radar detector with enhanced mismatched signals rejection capabilities," *EURASIP Journal on Advances in Signal Processing*, vol. 2010, no. 1, p. 375136, Nov 2010. [Online]. Available: <https://doi.org/10.1155/2010/375136>
- [4] W. Liu, W. Xie, and Y. Wang, "Parametric detector in the situation of mismatched signals," *IET Radar, Sonar Navigation*, vol. 8, no. 1, pp. 48–53, January 2014.
- [5] F. Bandiera and D. Orlando and G. Ricci, "A subspace-based adaptive sidelobe blanker," *IEEE Transactions on Signal Processing*, vol. 56, no. 9, pp. 4141–4151, Sep. 2008.
- [6] F. Bandiera, A. De Maio, and G. Ricci, "Adaptive CFAR radar detection with conic rejection," *IEEE Transactions on Signal Processing*, vol. 55, no. 6, pp. 2533–2541, June 2007.
- [7] F. Bandiera, D. Orlando, and G. Ricci, "CFAR detection strategies for distributed targets under conic constraints," *IEEE Transactions on Signal Processing*, vol. 57, no. 9, pp. 3305–3316, Sep. 2009.
- [8] F. Bandiera, O. Besson, D. Orlando, and G. Ricci, "An improved adaptive sidelobe blanker," *IEEE Transactions on Signal Processing*, vol. 56, no. 9, pp. 4152–4161, Sep. 2008.
- [9] N. B. Pulsone and M. A. Zatman, "A computationally efficient two-step implementation of the GLRT," *IEEE Transactions on Signal Processing*, vol. 48, no. 3, pp. 609–616, March 2000.
- [10] C. D. Richmond, "Performance of the adaptive sidelobe blanker detection algorithm in homogeneous environments," *IEEE Transactions on Signal Processing*, vol. 48, no. 5, pp. 1235–1247, May 2000.
- [11] C. D. Richmond, "Statistical performance analysis of the adaptive sidelobe blanker detection algorithm," in *Conference Record of the Thirty-First Asilomar Conference on Signals, Systems and Computers (Cat. No.97CB36136)*, vol. 1, Nov 1997, pp. 872–876 vol.1.
- [12] C. Hao, B. Liu, and L. Cai, "Performance analysis of a two-stage Rao detector," *Signal Processing*, vol. 91, no. 8, pp. 2141 – 2146, 2011. [Online]. Available: <http://www.sciencedirect.com/science/article/pii/S0165168411000806>
- [13] A. De Maio and D. Orlando, "Feature article: A survey on two-stage decision schemes for point-like targets in Gaussian interference," *IEEE Aerospace and Electronic Systems Magazine*, vol. 31, no. 4, pp. 20–29, April 2016.
- [14] F. Bandiera, D. Orlando, and G. Ricci, *Advanced Radar Detection Schemes Under Mismatched Signal Models*, ser. Synthesis Lectures on Signal Processing. Morgan & Claypool Publishers, 2009.
- [15] F. Bandiera, O. Besson, and G. Ricci, "An ABORT-Like Detector With Improved Mismatched Signals Rejection Capabilities," *IEEE Transactions on Signal Processing*, vol. 56, no. 1, pp. 14–25, Jan 2008.
- [16] J. Liu, K. Li, X. Zhang, M. Liu, and W. Liu, "A weighted detector for mismatched subspace signals," *Signal Processing*, vol. 140, pp. 110 – 115, 2017. [Online]. Available: <http://www.sciencedirect.com/science/article/pii/S0165168417301822>
- [17] A. De Maio, "Robust adaptive radar detection in the presence of steering vector mismatches," *IEEE Transactions on Aerospace and Electronic Systems*, vol. 41, no. 4, pp. 1322–1337, Oct 2005.
- [18] N. B. Pulsone and C. M. Rader, "Adaptive beamformer orthogonal rejection test," *IEEE Transactions on Signal Processing*, vol. 49, no. 3, pp. 521–529, March 2001.
- [19] A. De Maio, C. Hao, and D. Orlando, "Two-stage detectors for point-like targets in gaussian interference with unknown spectral properties," in *Modern radar detection theory*. SciTech Publishing Inc, 2016, ch. 4.
- [20] A. De Maio, S. De Nicola, Y. Huang, S. Zhang, and A. Farina, "Adaptive Detection and Estimation in the Presence of Useful Signal and Interference Mismatches," *IEEE Transactions on Signal Processing*, vol. 57, no. 2, pp. 436–450, Feb 2009.
- [21] E. J. Kelly, "An adaptive detection algorithm," *IEEE Transactions on Aerospace and Electronic Systems*, no. 2, pp. 115–127, 1986.
- [22] F. C. Robey, D. R. Fuhrmann, E. J. Kelly, and R. Nitzberg, "A CFAR adaptive matched filter detector," *IEEE Transactions on Aerospace and Electronic Systems*, vol. 28, no. 1, pp. 208–216, 1992.
- [23] A. De Maio, "Rao test for adaptive detection in Gaussian interference with unknown covariance matrix," *IEEE Transactions on Signal Processing*, vol. 55, no. 7, pp. 3577–3584, July 2007.
- [24] D. Orlando and G. Ricci, "A Rao test with enhanced selectivity properties in homogeneous scenarios," *IEEE Transactions on Signal Processing*, vol. 58, no. 10, pp. 5385–5390, Oct 2010.
- [25] J. Liu, W. Liu, B. Chen, H. Liu, H. Li, and C. Hao, "Modified Rao test for multichannel adaptive signal detection," *IEEE Transactions on Signal Processing*, vol. 64, no. 3, pp. 714–725, Feb 2016.
- [26] A. De Maio, D. Orlando, C. Hao, and G. Foglia, "Adaptive detection of point-like targets in spectrally symmetric interference," *IEEE Transactions on Signal Processing*, vol. 64, no. 12, pp. 3207–3220, June 2016.
- [27] J. Liu, G. Cui, H. Li, and B. Himed, "On the performance of a persymmetric adaptive matched filter," *IEEE Transactions on Aerospace and Electronic Systems*, vol. 51, no. 4, pp. 2605–2614, Oct 2015.
- [28] F. Bandiera, O. Besson, D. Orlando, G. Ricci, and L. L. Scharf, "GLRT-Based Direction Detectors in Homogeneous Noise and Subspace Interference," *IEEE Transactions on Signal Processing*, vol. 55, no. 6, pp. 2386–2394, June 2007.
- [29] F. Bandiera, A. De Maio, A. S. Greco, and G. Ricci, "Adaptive radar detection of distributed targets in homogeneous and partially homogeneous noise plus subspace interference," *IEEE Transactions on Signal Processing*, vol. 55, no. 4, pp. 1223–1237, April 2007.
- [30] S. Kraut, L. L. Scharf, and L. T. McWhorter, "Adaptive subspace detectors," *IEEE Transactions on Signal Processing*, vol. 49, no. 1, pp. 1–16, Jan 2001.
- [31] S. Kraut and L. L. Scharf, "The CFAR adaptive subspace detector is a scale-invariant GLRT," *IEEE Transactions on Signal Processing*, vol. 47, no. 9, pp. 2538–2541, Sep. 1999.
- [32] D. Adamy, *EW101: A First Course in Electronic Warfare*. Norwood, MA: Artech House, 2001.
- [33] D. L. Donoho, "Compressed sensing," *IEEE Transactions on Information Theory*, vol. 52, no. 4, pp. 1289–1306, April 2006.
- [34] J. A. Tropp and A. C. Gilbert, "Signal recovery from random measurements via orthogonal matching pursuit," *IEEE Transactions on Information Theory*, vol. 53, no. 12, pp. 4655–4666, Dec 2007.
- [35] D. L. Donoho, M. Elad, and V. N. Temlyakov, "Stable recovery of sparse overcomplete representations in the presence of noise," *IEEE Transactions on Information Theory*, vol. 52, no. 1, pp. 6–18, Jan 2006.

- [36] X. Tan, W. Roberts, J. Li, and P. Stoica, "Sparse learning via iterative minimization with application to MIMO radar imaging," *IEEE Transactions on Signal Processing*, vol. 59, no. 3, pp. 1088–1101, 2011.
- [37] M. Rossi, A. M. Haimovich, and Y. C. Eldar, "Spatial compressive sensing for MIMO radar," *IEEE Transactions on Signal Processing*, vol. 62, no. 2, pp. 419–430, Jan 2014.
- [38] D. Malioutov, M. Cetin, and A. S. Willsky, "A sparse signal reconstruction perspective for source localization with sensor arrays," *IEEE Transactions on Signal Processing*, vol. 53, no. 8, pp. 3010–3022, Aug 2005.
- [39] M. M. Hyder and K. Mahata, "Direction-of-Arrival Estimation Using a Mixed $\ell_{2,0}$ Norm Approximation," *IEEE Transactions on Signal Processing*, vol. 58, no. 9, pp. 4646–4655, Sep. 2010.
- [40] Z. Tan, Y. C. Eldar, and A. Nehorai, "Direction of Arrival Estimation Using Co-Prime Arrays: A Super Resolution Viewpoint," *IEEE Transactions on Signal Processing*, vol. 62, no. 21, pp. 5565–5576, Nov 2014.
- [41] Z. Liu, Z. Huang, and Y. Zhou, "An Efficient Maximum Likelihood Method for Direction-of-Arrival Estimation via Sparse Bayesian Learning," *IEEE Transactions on Wireless Communications*, vol. 11, no. 10, pp. 1–11, October 2012.
- [42] J. Zhang, D. Zhu, and G. Zhang, "Adaptive Compressed Sensing Radar Oriented Toward Cognitive Detection in Dynamic Sparse Target Scene," *IEEE Transactions on Signal Processing*, vol. 60, no. 4, pp. 1718–1729, April 2012.
- [43] S. Sen, "Low-Rank Matrix Decomposition and Spatio-Temporal Sparse Recovery for STAP Radar," *IEEE Journal of Selected Topics in Signal Processing*, vol. 9, no. 8, pp. 1510–1523, Dec 2015.
- [44] E. Conte, M. Lops, and G. Ricci, "Asymptotically optimum radar detection in compound-Gaussian clutter," *IEEE Transactions on Aerospace and Electronic Systems*, vol. 31, no. 2, pp. 617–625, April 1995.
- [45] A. Farina, *Antenna-Based Signal Processing Techniques for Radar Systems*. Boston, MA: Artech House, 1992.
- [46] —, *Electronic Counter-countermeasures*. McGraw-Hill, 2008, ch. 24.
- [47] M. Greco, F. Gini, A. Farina, and V. Ravenni, "Effect of phase and range gate pull-off delay quantisation on jammer signal," *IEE Proceedings - Radar, Sonar and Navigation*, vol. 153, no. 5, pp. 454–459, 2006.
- [48] J. S. Bergin, P. M. Techau, W. L. Melvin, and J. R. Guerci, "GMTI STAP in target-rich environments: site-specific analysis," in *Proceedings of the 2002 IEEE Radar Conference (IEEE Cat. No.02CH37322)*, April 2002, pp. 391–396.
- [49] L. Yan, P. Addabbo, C. Hao, D. Orlando, and A. Farina, "New ECCM techniques against noise-like and/or coherent interferers," *IEEE Transactions on Aerospace and Electronic Systems*, 2019, in print.
- [50] S. Han, C. Fan, and X. Huang, "A novel step based on spectrum-aided reduced-dimension clutter sparse recovery," *IEEE Geoscience and Remote Sensing Letters*, vol. 14, no. 2, pp. 213–217, 2017.
- [51] D. Needell and J. Tropp, "CoSaMP: Iterative signal recovery from incomplete and inaccurate samples," *Applied and Computational Harmonic Analysis*, vol. 26, no. 3, pp. 301–321, 2009.
- [52] T. Yardibi, J. Li, P. Stoica, M. Xue, and A. B. Baggeroer, "Source Localization and Sensing: A Nonparametric Iterative Adaptive Approach Based on Weighted Least Squares," *IEEE Transactions on Aerospace and Electronic Systems*, vol. 46, no. 1, pp. 425–443, Jan 2010.
- [53] C. Liu, L. Ding, and W. Chen, "A correction and generalization to the sparse learning via iterative minimization method for target off the grid in MIMO radar imaging," in *2012 Conference Record of the Forty Sixth Asilomar Conference on Signals, Systems and Computers (ASILOMAR)*. IEEE, 2012, pp. 895–899.
- [54] L. Xu, K. Zhao, J. Li, and P. Stoica, "Wideband source localization using sparse learning via iterative minimization," *Signal Processing*, vol. 93, no. 12, pp. 3504–3514, 2013.
- [55] M. Jabbarian-Jahromi and M. H. Kahaei, "Two-dimensional SLIM with application to pulse Doppler MIMO radars," *EURASIP Journal on Advances in Signal Processing*, vol. 2015, no. 1, p. 69, 2015.
- [56] P. Addabbo, A. Aubry, A. De Maio, L. Pallotta, and S. L. Ullo, "HRR profile estimation using SLIM," *IET Radar, Sonar & Navigation*, vol. 13, no. 4, pp. 512–521, 2018.
- [57] M. Feng, M. He, C. Chen *et al.*, "2-D DOA estimation using off-grid sparse learning via iterative minimization with L-parallel coprime array," *Chinese Journal of Electronics*, vol. 27, no. 6, pp. 1322–1328, 2018.
- [58] A. Aubry, V. Carotenuto, A. De Maio, and M. A. Govoni, "Multi-snapshot spectrum sensing for cognitive radar via block-sparsity exploitation," *IEEE Transactions on Signal Processing*, vol. 67, no. 6, pp. 1396–1406, March 2019.
- [59] M. A. Richards, J. A. Scheer, and W. A. Holm, *Principles of Modern Radar: Basic Principles*. Raleigh, NC: Scitech Publishing, 2010.
- [60] P. Stoica and Y. Selen, "Model-order selection: a review of information criterion rules," *IEEE Signal Processing Magazine*, vol. 21, no. 4, pp. 36–47, July 2004.
- [61] P. Stoica, Y. Selen, and J. Li, "On information criteria and the generalized likelihood ratio test of model order selection," *IEEE Signal Processing Letters*, vol. 11, no. 10, pp. 794–797, Oct 2004.
- [62] E. J. Candes and M. B. Wakin, "An introduction to compressive sampling," *IEEE Signal Processing Magazine*, vol. 25, no. 2, pp. 21–30, March 2008.



Sudan Han received the B.S. degree in information engineering, the M.S. and Ph.D. degrees in information and communication engineering, from the National University of Defense Technology, Changsha, China, in 2012, 2015 and 2019, respectively. She is currently an Assistant Researcher with the National Innovation Institute of Defense Technology, Beijing, China. Her main research interests include clutter suppression and target detection.



Luca Pallotta (S'12, M'15, SM'18) received the Laurea Specialistica degree (cum laude) in telecommunication engineering in 2009 from the University of Sannio, Benevento, Italy, and the Ph.D. degree in electronic and telecommunication engineering in 2014 from the University of Naples Federico II, Naples, Italy. He is currently an Assistant Professor at University of Roma Tre, Italy. His research interest lies in the field of statistical signal processing, with emphasis on radar/SAR signal processing, radar targets classification, polarimetric radar/SAR. Dr.

Pallotta won the Student Paper Competition at the IEEE Radar Conference 2013.



Xiaotao Huang (M'02) received the B.S. and Ph.D. degrees in information and communication engineering from the National University of Defense Technology, Changsha, China, in 1990 and 1999, respectively.

He is currently a Professor with the National University of Defense Technology. His fields of interest include radar theory, signal processing, and radio frequency signal suppression.



Gaetano Giunta (M'88, SM'12) received the Electronic Engineering degree from the University of Pisa, Italy, and the Ph.D. degree in Information and Communication Engineering from the University of Rome La Sapienza, Italy, in 1985 and 1990, respectively. He was also (since 1989) a Research Fellow of the Signal Processing Laboratory (LTS) at EPFL, Lausanne, Switzerland. In 1992, he became an Assistant Professor with the INFO-COM Department, University of Rome La Sapienza. From 2001 to 2005, he was with the Third University of

Rome as an Associate Professor. Since 2005, he has been a Full Professor of Telecommunications with the same University. His research interests include signal processing for mobile communications, image communications and security. Prof. Giunta has been a member of the IEEE Societies of Communications, Signal Processing, and Vehicular Technology. He has also served as a reviewer for several IEEE transactions, IET (formerly IEE) proceedings, and EURASIP journals, and a TPC member for several international conferences and symposia in the same fields.



Danilo Orlando (SM'13) was born in Gagliano del Capo, Italy, on August 9, 1978. He received the Dr. Eng. Degree (with honors) in computer engineering and the Ph.D. degree (with maximum score) in information engineering, both from the University of Salento (formerly University of Lecce), Italy, in 2004 and 2008, respectively. From July 2007 to July 2010, he has worked with the University of Cassino (Italy), engaged in a research project on algorithms for track-before-detect of multiple targets in uncertain scenarios. From September to

November 2009, he has been visiting scientist at the NATO Undersea Research Centre (NURC), La Spezia (Italy). From September 2011 to April 2015, he has worked at Elettronica SpA engaged as system analyst in the field of Electronic Warfare. In May 2015, he joined Universit degli Studi "Niccolò Cusano", where he is currently associate professor. His main research interests are in the field of statistical signal processing and image processing with more emphasis on adaptive detection and tracking of multiple targets in multisensor scenarios. He has held visiting positions at the department of Avionics and Systems of ENSICA (now Institut Supérieur de l'Aéronautique et de l'Espace, ISAE), Toulouse (France) in 2007 and at Chinese Academy of Science, Beijing (China) in 2017-2019.

He is Senior Member of IEEE; he has served IEEE Transactions on Signal Processing as Senior Area Editor and currently is Associate Editor for IEEE Open Journal on Signal Processing, EURASIP Journal on Advances in Signal Processing, and MDPI Remote Sensing. He is also author or co-author of about 110 scientific publications in international journals, conferences, and books.